nature portfolio

https://doi.org/10.1038/s41586-026-11180-5

Supplementary information

Stone and water governed early human settlement of the desert

In the format provided by the authors and unedited

Supplementary Information for "Stone and water governed early human settlement of the desert" Dellmour et al.

Contents

1. Quaternary Facies
2. Palaeohydrology
3. Correlation with published palaeolakes
4. Oman archaeological survey data
5. Spatial modelling of human occupation potential
6. Chronology of palaeolakes and archaeological sites
7. Colonisation dynamics in dual-resource landscapes
8. Future research and strategies
9. References

1. Quaternary Facies

The Rub' al Khali crossing expedition documented Quaternary surface facies at 125 localities along the transect (Supplementary Data 1; Fig. S1). These observations form the empirical basis for the geological assessment of lithic raw material availability presented in the main text. Five main types of sedimentary facies, including rare bedrock outcrops embedded in and partially covered by aeolian sands, were recorded and grouped as: (1) Cretaceous & Eocene bedrock outcrops; (2) fluvial–alluvial gravel and debris; (3) lacustrine limestones and shales (freshwater); (4) lacustrine dolomitic microbial build-ups (saline/hypersaline); (5) sabkha (evaporitic). The distribution of these facies along the transect reflects the regional Quaternary stratigraphic architecture of the Rub' al Khali basin, in which Mesozoic–Eocene formations containing chert-bearing lithologies dip eastward beneath a thick sequence of Neogene to Quaternary siliciclastic, carbonatic, and evaporitic basin fill[29,30], forming a large structural syncline below the central Rub' al Khali. These lithologies reach the surface again at the eastern end of the transect.

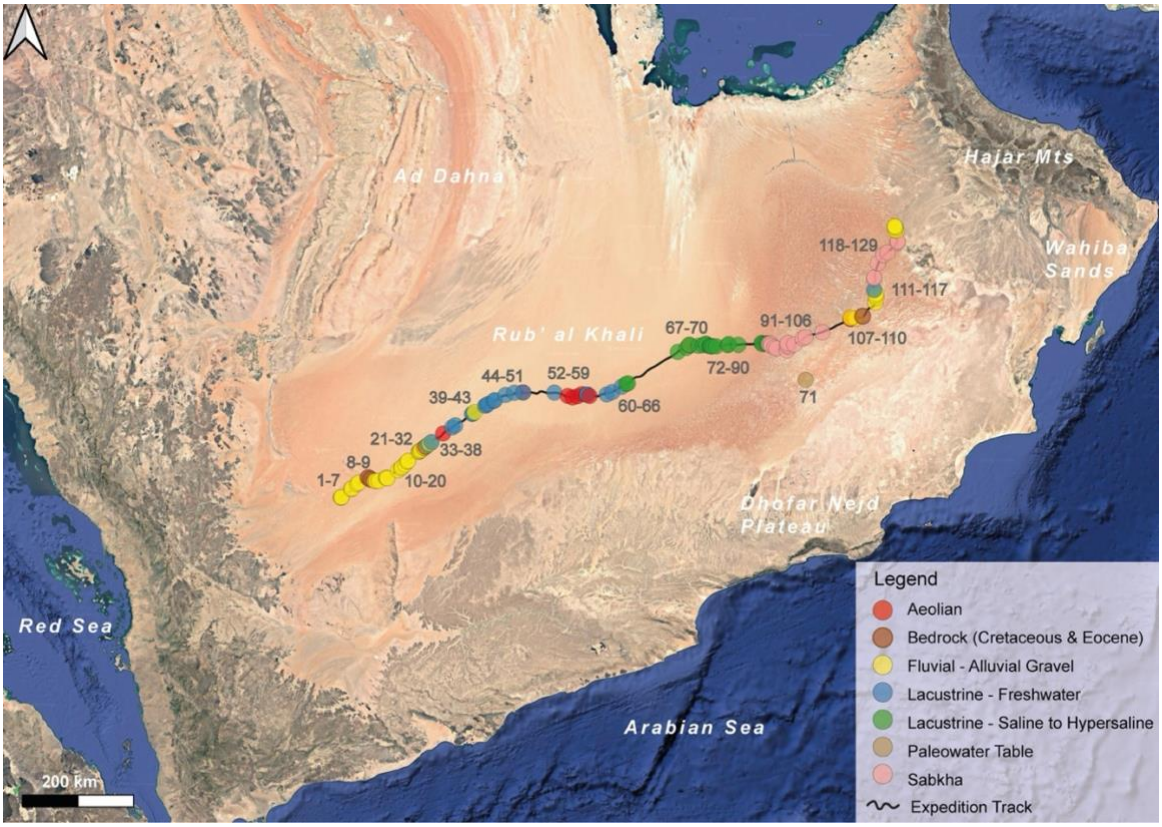

Fig. S1 | Quaternary facies distribution along the Rub' al Khali crossing transect. Coloured symbols indicate dominant surface facies recorded at 125 localities: bedrock outcrops (Lower Cretaceous Wasia and Eocene Dammam formations; brown), fluvial–alluvial gravel (yellow), freshwater lacustrine deposits (blue), exhumed palaeo water-table (tan), saline to hypersaline microbial build-ups (green), and sabkha evaporites (pink) and aeolian sand (red). The surveyed route runs ~1,500 km from the Mundafan palaeolake basin (southwest) to the Hajar mountain piedmont (northeast). No knappable lithic raw material was recorded at any locality between the Wasia Formation outcrops (~46.8°E) and the Dammam Formation exposures (~54.7°E), an interval of ~800 km. Map produced in QGIS 3.28; base imagery © Google.

1.1 Western margin (Sites 1-9; ~46.3°-46.8°E)

The transect begins in the vicinity of the Mundafan palaeolake basin, where isolated outcrops of Jurassic Hanifa Formation are flanked by siliciclastic gravels of fluvial-alluvial origin. Surface lithologies at these localities are dominated by lag deposits overlying older fluvial units, consistent with the distal extent of Wadi ad Dawasir's alluvial system[33,67]. The westernmost palaeolake deposits (Sites 2, 5-7) consist of limestone and gypcrete in lacustrine freshwater settings, with *Melanoides tuberculata* and ostrich eggshell fragments recorded at several localities. Approximately 80 km northeast of Mundafan, Sites 8 and 9 expose outcrops of the Lower Cretaceous Wasia Formation (Fig. S2). These yielded heavily weathered silicified sandstones, the only bedrock-derived lithic raw material encountered on the western half of the transect. East of these outcrops, Mesozoic formations dip beneath the Neogene-Quaternary basin fill and no further bedrock exposures were observed until the eastern margin of the desert.

Fig. S2 | Lithic raw material occurrences along the Rub' al Khali crossing transect | (a) Heavily weathered silicified sandstone of the Lower Cretaceous Wasia Formation at the westernmost bedrock exposures (Sites 8 and 9, ~46.8°E), representing the only knappable bedrock encountered on the western half of the transect. **(b)** Siliciclastic gravels with mixed lithologies at Site 34 (~48°E), characteristic of deflated fluvial-alluvial lag surfaces in the western-central interior; no clasts of knappable quality were observed. **(c)** In situ chert nodules weathering out of Eocene Dammam Formation carbonates on the eastern margin (~54.9°E), the first bedrock-derived knappable lithology east

of the Wasia outcrops and ~800 km from them. **(d)** Rounded to sub-rounded chert clasts of the Miocene Dam Formation (Fars Group) dispersed across the Umm as Samim basin, reworked from Late Cretaceous obducted ophiolitic nappes. All chert and silicified sandstone shown are naturally occurring geological materials, either in situ nodules or fluvially reworked clasts; none bear intentional flaking attributes and no artefacts were identified at any locality. Hammer (33 cm) and hand lens (5 cm) for scale.

1.2 Western interior (Sites 10-47; ~47.0°-48.9°E)

East of the Wasia outcrops, the transect enters the dune-dominated interior. Interdunal exposures in this zone are characterised by two facies associations. The first comprises siliciclastic gravel lags and mixed gravel-dune surfaces, representing deflated remnants of older fluvial-alluvial deposits overlain by aeolian sands. The second consists of freshwater palaeolake deposits, recorded at 11 localities in this section as beige micritic limestones and gypcretes The "limestone facies" described by Matter et al.[16] consisting of beige micrites up to 270 cm thick with bioturbation and abundant *M. tuberculata* and *C. fluminalis*, corresponds to the survey's freshwater limestone facies. *M. tuberculata* is common in Arabian freshwater springs and oases but also occurs in brackish desert springs up to about 9 ppt[68,69], while *C. fluminalis* indicates persistent freshwater to oligohaline conditions and disappears above roughly 5 ppt[70,71]. Both are therefore indicators of persistent aquatic habitat rather than potable water. Across the transect as a whole, freshwater limestone and gypcrete were recorded at 21 localities, and dolomitic and gypsiferous microbial build-ups, described in Section 1.3, at a further 27. Both facies are exclusively associated with elevated groundwater levels and the formation of palaeolake deposits up to several metres thick. Palaeolake evidence was recorded at 55 localities in total, comprising these primary lacustrine facies together with four localities where lacustrine carbonate occurs as reworked debris within alluvial gravels, three exhumed palaeowater table surfaces, and one where lacustrine material is preserved within aeolian sands. Unlike the Mundafan lake, which was fed primarily by wadi inflow into a regional depression[7,10], the western interior palaeolakes were groundwater-fed systems lacking fluvial connectivity. Neither facies contain lithologies suitable for stone tool manufacture.

1.3 Central interior and salt lake zone (Sites 48-90; ~49.0°-53.0°E)

The central portion of the transect traverses the lowest elevations of the basin, where active and palaeosabkha deposits become the dominant surface facies. Active salt lakes (n = 13) with halite crusts and brine pools occur in the 'Uruq al-Mu'taridah depression, where the groundwater table lies within 1-2 m of the surface. These are flanked by extensive evaporitic sabkha flats (n = 20) characterised by gypcrete pavements, gypsum rosettes, and lenticular gypsum crystals—the characteristic "sabkha facies" of Matter et al.[16]. Exhumed palaeowater table surfaces (n = 3) are preserved as carbonate-encrusted former capillary fringes within palaeodune sands, recording the position of the water table during past humid intervals (Supplementary Information Section 2). The sedimentary lithologies throughout this zone are exclusively carbonatic and evaporitic. No

siliceous bedrock, transported siliceous clasts, or chert-bearing formations were observed at any locality.

1.4 Eastern margin (Sites 91-129; ~53.3°-55.5°E)

The eastern margin of the transect encompasses the Umm as Samim, a large endorheic sabkha basin at the northeastern terminus of the Rub' al Khali that receives drainage from the Hajar mountain front. The transect exits the dune fields onto a Quaternary distal fan surface comprising siliciclastic gravels and consolidated aeolian sands (n = 6). East of the basin, alluvial gravels containing carbonatic clasts (n = 4) become progressively more common. Knappable raw material reappears at Site 107 (~54.7°E) in the form of fluvially transported chert gravels. Site 111 exposes in situ Eocene Dammam Formation carbonates containing chert nodules, which are the first bedrock-derived knappable lithology encountered since the Wasia Formation outcrops ~800 km to the west. From Site 107 eastward to the end of the transect at Site 129, eight of 23 localities yielded knappable raw material, all within Dam Formation-derived alluvial gravels or Dammam Formation exposures.

The chert gravels redistributed into the Umm as Samim basin are most plausibly sourced from the Miocene Dam Formation of the Fars Group. The Dam Formation contains chert clasts ultimately derived from the obducted ophiolitic nappes across northern Oman during the Late Cretaceous, subsequently uplifted and reworked during Late Cenozoic tectonic phases associated with the Oman Mountains and redistributed across interior basins including Umm as Samim. Because this chert has undergone multiple phases of transport, uplift, and redeposition, it occurs as rounded to sub-rounded clasts rather than fresh in situ nodules, and is of variable but generally knappable quality. This material is not transported southwest beyond Umm as Samim and therefore provides no source of knappable raw material for the central Rub' al Khali interior.

1.5 Summary of survey results

Of 125 documented localities, knappable lithic raw material was present at only 10 (8%), restricted entirely to the western and eastern margins of the transect: two Wasia Formation outcrops at ~46.7°-46.8°E and eight eastern margin localities at ~54.7°-55.2°E (one Dammam Formation bedrock exposure and seven alluvial gravels carrying reworked Dam Formation chert). Across the intervening ~800 km of the interior Rub' al Khali basin, surface lithologies consist exclusively of carbonatic, evaporitic, and siliciclastic (quartz sand) facies, none of which possess the conchoidal fracture properties required for stone tool manufacture. This distribution is a direct consequence of the basin's stratigraphy: the Palaeocene–Eocene chert-bearing formations (Umm Er Radhuma, Rus, and Dammam Formations) that crop out at the basin margins are progressively buried beneath Neogene–Quaternary basin fill toward the interior (Fig. 4b). Furthermore, the groundwater-fed character of interior palaeolakes (Supplementary Information Section 2) precluded fluvial transport of siliceous clasts from distant highland sources, making fluvial introduction of knappable material into the central basin unlikely.

2. Palaeohydrology

Direct sedimentary evidence confirms that interior palaeolakes were groundwater-fed systems lacking fluvial connectivity. Along the entire 1,500 km transect, no fluvial sediment input into the palaeolake depressions was observed. Any contemporaneous fluvial environments in adjacent areas, given their proximity to the topographically low palaeolake basins, would have produced diagnostic sedimentary signatures such as coarse clastic input, gravel lenses, or current-generated structures, none of which were recorded at any locality. Fluvial and alluvial sediments were observed only at the western and eastern ends of the transect, in neither case in stratigraphic association with palaeolake deposits.

Exhumed palaeowater table surfaces provide positive evidence for groundwater discharge. All observed outcrops of palaeowater tables occur exclusively within the zone of dolomitic–gypsiferous microbial build-ups in the central portion of the transect (Fig. S1). These surfaces are preserved as carbonate-encrusted former capillary fringes within palaeodune sands (Fig. S3), recording the position of the water table during past humid intervals. The present-day water table is substantially lower: at the approximate location 19.108°N, 50.112°E (*Umm al Melh*, "mother of salt"), groundwater was reported at ~63 m depth in a freshwater well (S. al Melh, pers. comm., 23 November 2023), consistent with modern hydrogeological assessments showing deep water tables across the central Rub' al Khali interior[72,73].

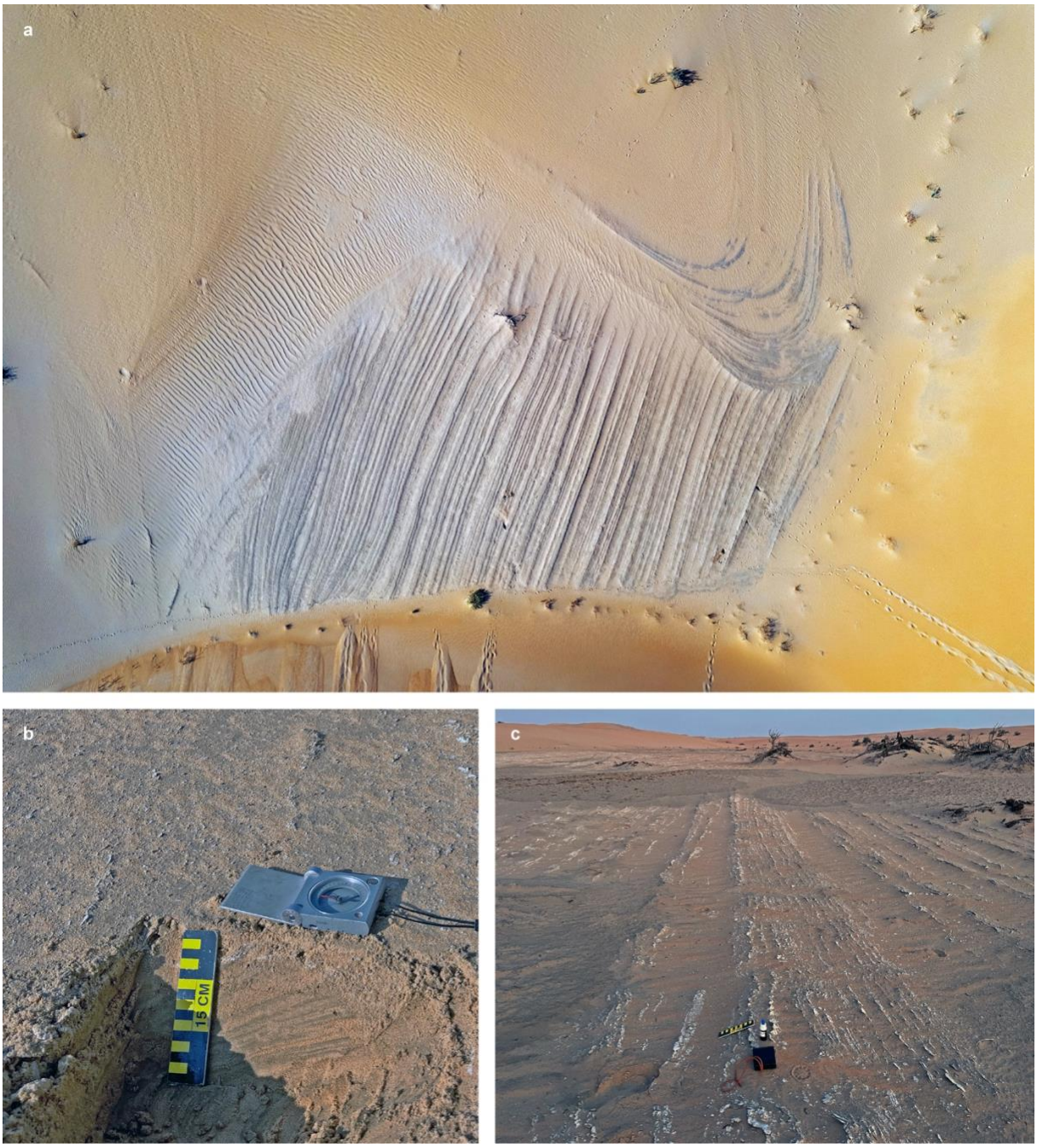

Fig. S3 | Exhumed palaeowater table at 20.315°N, 52.063°E. (a) Aerial view (fox tracks for approximate scale in lower right). The exposed surface marks the former capillary fringe within a palaeodune, preserved by carbonate encrustation at the air–water interface. E–W-trending linear features are south-dipping cross-strata (strike/dip: 170/32°); parabolic laminae dipping <5° SW indicate a prevailing northerly to northeasterly palaeowind direction. Overlying aeolian sands were removed by deflation, exposing this surface. **(b)** Detail showing mm-scale stratification of palaeodune sands deposited prior to exhumation of palaeowater table; darker laminae are heavy-mineral-enriched bases of individual aeolian cycles (confirmed by magnetic test). Scale bar: 15 cm, compass is oriented North (right) - South (left). **(c)** Ground-level view toward east showing the lateral extent of the exhumed surface. Several palaeolake deposits documented during the 2023 survey overlie comparable exhumed palaeowater table surfaces, consistent with observations at Mundafan[7]. Drone photography: T. Bresenhuber 2023.

3. Correlation with published palaeolakes

This section documents the spatial and stratigraphic relationship between palaeolake localities surveyed during the Rub' al Khali crossing expedition and the independently dated lake deposits published by Matter et al.[16]. The correlation provides the basis for the chronological framework in the archaeological observations.

3.1 Topographic and hydrological context

The interior Rub' al Khali comprises a series of shallow, groundwater-fed lake basins arranged along regional drainage gradients that slope from the Arabian Shield toward the Sabkha Matti lowlands in the northeast. Palaeolake deposits in the surveyed transect occur at progressively lower elevations from west to east, reflecting this regional topographic structure. The relationship between longitude and elevation across all documented palaeolake localities is highly linear (adjusted $R^2 = 0.913$, $P < 0.001$), with elevation decreasing approximately 71.7 m per degree of longitude eastward (Extended Data Fig. 3). This consistent gradient indicates that the surveyed palaeolakes occupy positions within a coherent hydrological system rather than isolated, unrelated depressions.

Groundwater recharge during humid phases was derived from the Asir Mountains and Arabian Shield to the west, with flow directed through regional aquifer systems toward the interior basins[73,74]. Hydrogeological studies document this east-directed subsurface flow pattern[75], which explains both the systematic elevation gradient and the groundwater-fed (phreatic) character of the lacustrine deposits, as evidenced by their distinctive carbonatic lithology, absence of fluvial and deltaic facies, and presence of freshwater mollusc assemblages.

3.2 Elevation-based stratigraphic correlation

Lake deposits at equivalent elevations within the same hydrological basin are conventionally interpreted to represent coeval lake stands[76,77], although equivalent elevation alone is not sufficient to demonstrate coevality, particularly across deflated and groundwater-fed systems. This approach provides the basis for correlating the survey localities to the previously dated sections, supported by multiple lines of evidence: (1) survey localities in the eastern interior (Sites 61 to 65) occur within 6 to 31 km of luminescence-dated sections; (2) localities at equivalent distance along the regional gradient exhibit consistent elevation ranges (typically ±20 m, within the expected variance for coeval lake deposits subject to differential post-depositional deflation); and (3) sedimentary facies at survey localities are consistent with those described at dated sections, including bioturbated limestone layers, carbonate platforms with microbial build-ups, and freshwater mollusc assemblages dominated by *M. tuberculata*.

Tables S1 and S2 and Extended Data Fig. 3 present the correlation between the palaeolake sections of Matter et al.[16] and the survey localities documented during the Rub' al Khali crossing expedition. Table S1 lists the sections used as the chronological framework, distinguishing those dated by luminescence from those observed but not dated. Table S2 lists the 24 surveyed

palaeolake localities that fall within the longitudinal span of the dated and observed sections, between 47.72 and 51.04 degrees east, together with each locality's nearest Matter et al.[16] section with published coordinates, survey duration, evidence recorded, and the great-circle distance to that section. The remaining 31 palaeolake localities lie west (n = 3) or east (n = 28) of this span, where no published section provides a correlation anchor, and are listed in Supplementary Data 1. Coordinates and elevations of the Matter et al.[16] sections were extracted from the published figures. Survey-locality elevations derived from SRTM 30m DEM.

Table S1 | Luminescence-dated and observed palaeolake sections of Matter et al.[16] in the central Rub' al Khali, used as the chronological framework for the survey correlation.

Section	Latitude (°N)	Longitude (°E)	Elevation (m a.s.l.)	OSL age(s) (ka)	MIS stage	Dating status
11.2	18.51180	47.85305	526	–	–	Observed, not dated
12.2	18.77038	48.89435	399	–	–	Observed, not dated
13.1	19.29095	50.16006	274	73 ± 4	5a	OSL-dated (pIR-IRSL)
14.3	19.44267	51.03957	226	122 ± 6, 118 ± 10, 111 ± 9	5e–5d	OSL-dated (pIR-IRSL)
14.7	19.59215	50.71008	252	67 ± 9	5a–4	OSL-dated (pIR-IRSL)
14.9	19.68017	50.63062	230	–	–	Observed, not dated
15.1	19.43815	50.81028	241	107 ± 13	5c	OSL-dated (pIR-IRSL)
15.3	19.44405	50.78227	222	96 ± 6	5c	OSL-dated (pIR-IRSL)

OSL ages are post-IR IRSL (pIR-IRSL) determinations from Matter et al.[16] Table 1; site 14.3 yielded three determinations. Sections 11.2, 12.2 and 14.9 were described but not dated.

Table S2 | Surveyed palaeolake localities of the Rub' al Khali crossing expedition and their correlation to the sections in Table S1, ordered west to east. Listed here are the 24 palaeolake localities falling within the longitudinal span of those sections; the remaining 31 are given in Supplementary Data 1.

Locality	Latitude (°N)	Longitude (°E)	Elevation (m a.s.l.)	Nearest Matter et al. (2015) section	OSL age (ka)	MIS stage	Distance (km)	Survey duration (min)	Evidence
33	18.7511	47.7194	511	11.2	undated	–	30.1	20	O
34	18.7819	47.7605	505	11.2	undated	–	31.6	10	–
35	18.8046	47.7913	492	11.2	undated	–	33.2	drive-through	–
36	18.9366	47.9802	486	11.2	undated	–	49.1	drive-through	–
37	19.0317	48.1300	451	11.2	undated	–	64.7	300	O
38	19.0650	48.1833	443	11.2	undated	–	70.7	60	M
39	19.2428	48.4635	399	12.2	undated	–	69.4	60	–
40	19.2500	48.4753	399	12.2	undated	–	69.2	60	M
43	19.3692	48.6755	375	12.2	undated	–	70.4	60	M
44	19.3843	48.7039	373	12.2	undated	–	71.1	60	M
45	19.3975	48.7247	371	12.2	undated	–	72.0	300	M, O
46	19.4467	48.8217	351	12.2	undated	–	75.6	60	M
47	19.4570	48.8387	352	12.2	undated	–	76.6	15	M, O

Locality	Latitude (°N)	Longitude (°E)	Elevation (m a.s.l.)	Nearest Matter et al. (2015) section	OSL age (ka)	MIS stage	Distance (km)	Survey duration (min)	Evidence
48	19.5372	49.0145	333	12.2	undated	–	86.2	120	M
51	19.5743	49.1606	340	12.2	undated	–	93.7	300	M, O
50	19.5795	49.3112	335	13.1	73 ± 4	5a	94.6	300	M, O
52	19.5771	49.8232	285	13.1	73 ± 4	5a	47.5	30	M, O
59	19.5438	50.3671	252	14.9	undated	–	31.5	10	–
58	19.5461	50.3681	269	14.9	undated	–	31.3	10	–
61	19.5454	50.6905	252	14.7	67 ± 9	5a–4	5.6	10	M
62	19.5845	50.7819	238	14.7	67 ± 9	5a–4	7.6	120	M
63	19.6669	50.9399	236	14.7	67 ± 9	5a–4	25.5	120	M
64	19.7093	51.0136	218	14.3	122, 118, 111	5e–5d	29.8	120	–
65	19.7208	51.0445	224	14.3	122, 118, 111	5e–5d	30.9	30	–

Nearest section denotes the closest Matter et al.[16] section with published coordinates; distance is the great-circle distance to that section. Localities 61 and 62 lie within 8 km, and 63 to 65 within 31 km, of luminescence-dated sections (14.7, 14.3), providing direct chronological control. The remaining localities are correlated to the same MIS 5 palaeolake system by shared lacustrine facies and position on the regional piezometric gradient (Extended Data Fig. 3). For most of these, the nearest section with published coordinates is itself undated (11.2, 12.2, 14.9). Localities 50 and 52 lie nearest to section 13.1, which is dated to 73 ± 4 ka, but at 94.6 and 47.5 km respectively they are too distant from it to provide direct chronological control.

OSL age / MIS stage: age(s) and marine isotope stage of the nearest section where luminescence-dated; “undated” where the nearest located section was not dated (see Table S1).

Evidence: M, freshwater molluscs (*Melanoides tuberculata*, *Corbicula fluminalis*); O, ostrich eggshell. An en dash denotes localities at which neither was recorded. No lithic artefacts and no knappable raw material were recorded at any locality listed here.

Survey duration: time spent on foot at each locality, in minutes. "Drive-through" denotes localities assessed from the vehicle where exposure was limited or access constrained.

3.3 Sedimentary facies correlation

The lacustrine deposits at survey localities exhibit the same diagnostic facies described by Matter et al.[16] at their dated sections: grey to buff laminated marls deposited in shallow standing water; indurated carbonate platforms representing phreatic discharge zones; microbial build-ups (stromatolitic structures) indicating prolonged stable water levels; and freshwater mollusc assemblages dominated by *M. tuberculata* and *C. fluminalis*. The consistent facies architecture across all localities supports their interpretation as deposits of the same regional lake system active during MIS 5 humid intervals.

3.4 Uncertainty assessment

Several sources of uncertainty affect the correlation: (1) SRTM DEM vertical accuracy is ±5-10 m in flat terrain; (2) post-depositional deflation of exposed lacustrine surfaces may have lowered original shoreline elevations by 1-5 m; (3) lake levels oscillated within humid phases, producing lake deposits across elevation ranges of 10-20 m at any given time. The observed elevation ranges within each geographic cluster (typically 20 to 35 m within local clusters) are consistent with these combined uncertainties and with expected shoreline variability during lake highstands. Direct chronological control is provided by the eastern surveyed localities (Sites 61 to 65), which lie 6 to 31 km from dated sections 14.3 and 14.7 (Table S2), with Sites 61 and 62 within 8 km of dated section 14.7. Localities further west lie beyond the dated sections and are correlated to the same lake system by shared facies and their position on the regional piezometric gradient (Extended Data Fig. 3). Elevation differentials between surveyed localities and their nearest reference section scale with the distance separating them, as expected where both lie on a regional piezometric gradient. Among the six localities correlated to section 11.2, differentials of 15, 21, 34, 40, 75 and 83 m correspond to separations of 30.1, 31.6, 33.2, 49.1, 64.7 and 70.7 km, a linear relationship of 1.54 m per km ($R^2 = 0.950$) consistent with the gradient of 1.39 m per km computed independently across the same localities and with the transect-wide relationship in Extended Data Fig. 3. The largest differentials therefore occur at the greatest separations and reflect gradient rather than correlation error. Section 11.2 is in any case undated, so none of these localities contributes to the chronological framework, which rests on localities 61 to 65 at 5.6 to 31 km from the luminescence-dated sections 14.7 and 14.3.

4. Oman archaeological survey data

4.1 Overview of survey programme

The archaeological site database used in Extended Data Fig. 1 derives from 44 field expeditions conducted across Oman between 2002 and 2024 by J.I.R. (Table S3). These campaigns encompassed reconnaissance surveys (n = 4), research-driven investigations (n = 13) and commercial environmental impact assessments (n = 27; EIAs), collectively providing geographic coverage across six governorates throughout the country: Dhofar, Dakhliyah, Wusta, Dhahirah, Sharqiyah, and Musandam. Research campaigns focused primarily on the Dhofar Nejd plateau and adjacent regions under permits issued by the Ministry of Heritage and Tourism, Sultanate of Oman (formerly Ministry of Heritage and Culture). EIA campaigns were contracted by development companies and conducted across diverse regions of the country, often in areas not targeted by research programmes. This combination of research and commercial survey provides broader geographic representation than either would alone and reduces sampling bias. The distribution of surveyed localities and the occurrence of knappable raw material at each are shown in Fig. S4.

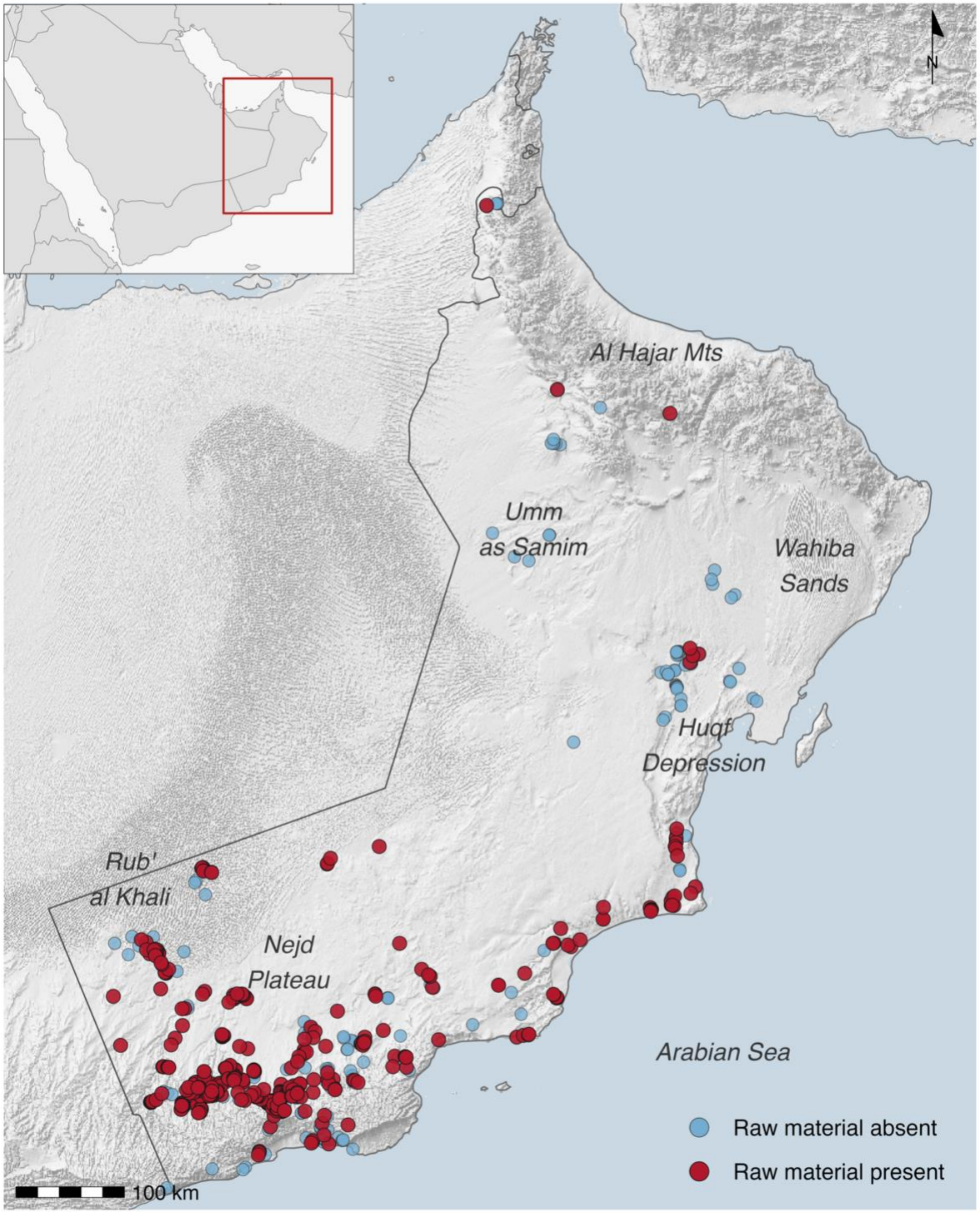

Fig. S4 | Raw material occurrence across the Oman survey programme. Survey localities recorded between 2002 and 2024 (Table S3), classified by the presence or absence of knappable lithic raw material. Filled red symbols denote localities at which knappable raw material was recorded; blue symbols denote localities at which no knappable raw material was present. Base map: GEBCO 2026 bathymetry and topography, illuminated from the northwest; coastlines and national boundaries from Natural Earth.

Table S3 | Archaeological survey campaigns in Oman, 2002–2024. Summary of 44 field campaigns contributing to the archaeological site database used in Extended Data Fig. 1.

Date	Governorate(s)	Area(s) surveyed	Type	Ref.
2002, July	Dhofar, Dakhliyah	Dhofar mountains, eastern Nejd plateau, northern Wahiba desert, Hajar mountain piedmont	Reconnaissance	78
2003, December	Dhofar, Dakhliyah	northern Huqf depression, Hajar mountain piedmont, eastern Nejd plateau	Research	79,80
2004, Jan - Mar	Dhofar, Wusta, Dakhliyah	eastern Nejd plateau, Duqm escarpment, northern Huqf depression, Qarat al Kibrit salt dome	Research	79–81
2006, May	Dhofar	Hajar mountain piedmont	Reconnaissance	—
2007, April	Dhofar, Dakhliyah	Wadi Tanuf, Ras Ain Noor	Research	81
2007, September	Dhofar	Al Hatab rockshelter	Research	81,82
2007, September	Dhahirah	Hamra ad Duru foothills	EIA	Unpub.
2007, December	Musandam	Ras al Jebel mountains	Research	Unpub.
2008, January	Dhofar	Al Hatab rockshelter	Research	81,82
2009, October	Dhofar	Salalah plain, Nejd plateau	Reconnaissance	—
2010, Jan - Mar	Dhofar	Salalah plain, Dhofar mountains, Nejd plateau, Aybut Auwal	Research	20,82–84
2010, April	Dakhliyah	northern Huqf depression	EIA	Unpub.
2011, Jan - Mar	Dhofar	Salalah plain, Dhofar mountains, Nejd plateau	Research	20,21,48,85
2012, Jan - Mar	Dhofar	Salalah plain, Dhofar mountains, Nejd plateau, southern Rub' al Khali desert	Research	20,21,83,84
2012, July	Dakhliyah	northern Huqf depression	EIA	Unpub.
2012, September	Dhahirah	Umm as Samim sabkha	EIA	Unpub.
2012, October	Dakhliyah	northern Huqf depression	EIA	Unpub.
2013, Jan - Mar	Dhofar	western Nejd plateau, southern Rub' al Khali desert, Matafah	Research	48,83,85–87
2014, April	Dakhliyah, Wusta	Huqf depression, Jiddat al Harassis plain	EIA	Unpub.
2014, April	Dhofar	eastern Nejd plateau	EIA	Unpub.
2014, September	Dhofar	southern Rub' al Khali desert	EIA	Unpub.
2014, October	Dakhliyah	northern Huqf depression	EIA	Unpub.
2014, November	Dakhliyah, Sharqiyah	northern Huqf depression, Bar al Hikman lagoon	EIA	Unpub.

2015, February	Dakhliyah	central Huqf depression	EIA	Unpub.
2015, July	Dhofar, Wusta	southeastern Nejd plateau, Jazer plain	EIA	Unpub.
2015, October	Dhofar	western Nejd plateau	EIA	Unpub.
2016, June	Dakhliyah	northern Huqf depression	EIA	Unpub.
2016, October	Dakhliyah, Dhahirah	northern Huqf depression, western Hajar mountain piedmont	EIA	Unpub.
2016, November	Dakhliyah	central Huqf depression	EIA	Unpub.
2017, May	Wusta	southern Huqf depression	EIA	Unpub.
2019, January	Sharqiyah	southern Ja'alan coast, Wahiba desert	EIA	Unpub.
2019, January	Dhofar	southern Rub' al Khali desert	EIA	Unpub.
2019, October	Sharqiyah	southern Ja'alan coast	EIA	Unpub.
2020, April	Dhofar	southern Nejd plateau	Reconnaissance	Unpub.
2021, February	Dhofar	southern Rub' al Khali desert	EIA	Unpub.
2021, March	Dhahirah	western Hajar mountain piedmont	EIA	Unpub.
2021, April	Wusta	southern Huqf depression, Jazer plain, Jiddat al Harassis plain	EIA	Unpub.
2021, June	Dhofar	southern Rub' al Khali desert	Research	In review
2021, June	Dhofar	eastern Nejd plateau	EIA	Unpub.
2022, Jan - Feb	Dhofar	southern Rub' al Khali desert, western Nejd plateau	Research	5
2022, April	Wusta	southern Huqf depression, Jazer plain, Jiddat al Harassis plain	EIA	Unpub.
2022, October	Dhahirah	western Hajar mountain piedmont	EIA	Unpub.
2023, Jan - Feb	Dhofar	southern Rub' al Khali desert, western Nejd plateau	Research	5
2024, January	Dhahirah	western Hajar mountain piedmont	EIA	Unpub.

The cumulative dataset comprises >1,200 lithic findspots spanning the Lower Palaeolithic through Neolithic, of which the MP/MSA component used in Extended Data Fig. 1 is drawn. Coordinates for all findspots were recorded using handheld GPS (typical accuracy ±5 m). The dataset has been compiled in GIS software and georeferenced against 1:250,000 geological mapping[88]. A published subset of the survey data appears in Rose et al.[83].

4.2 Survey methodology

Survey methods varied across campaigns in response to research objectives, landscape conditions, and logistical constraints. Three primary approaches were employed:

Systematic pedestrian survey. During dedicated research campaigns, transects were walked by surveyors spaced approximately 10 m apart, typically oriented perpendicular to wadi channels to sample site distributions relative to drainage systems. Transects ranged from 1 to 5 km in length and were positioned to sample the full range of geomorphic and ecological zones within the survey region.

Driving reconnaissance. Extensive areas were surveyed by vehicle along wadi systems, gravel plains, and desert tracks, with stops for pedestrian inspection at exposures of geological or archaeological interest. This approach maximised geographic coverage across the expansive Omani landscape and was particularly effective for identifying raw material outcrops and documenting the presence or absence of lithic material in relation to surface geology.

Environmental impact assessment. EIA surveys were conducted within defined concession areas to professional standards as required by the contracting authority, with survey intensity calibrated to available time and concession size. All EIA fieldwork was conducted by J.I.R. and adhered to International Finance Corporation (IFC) Performance Standard 8, ensuring consistent identification criteria and recording systems across the combined dataset.

The deflationary landscapes that characterise much of the Omani interior provide exceptional archaeological visibility. Across the Nejd plateau, the Jiddat al Harasis, and deflated interdunal surfaces, ground visibility typically exceeds 95%, supporting the inference that the absence of lithic material from surveyed localities is unlikely to be solely a preservation or visibility bias.

4.3 Survey coverage and potential bias

Survey coverage is distributed across the accessible terrain of central and southern Oman (Fig. S4), including extensive areas in which no knappable raw material was recorded. The pattern is not an artefact of selective survey: localities lacking raw material were documented at the same intensity as those where it occurs, and the concentration of raw-material occurrences along the Dhofar Nejd plateau and the eastern escarpments reflects the underlying geology rather than differential survey effort.

The dataset's heterogeneous origins, having been accumulated over two decades through campaigns with varying objectives, durations, and intensities, provide broader geographic and geological coverage than any single research programme could achieve. EIA campaigns were frequently situated on geological formations lacking knappable raw materials (e.g., Quaternary alluvium in Dakhliyah, gravel plains on the Jiddat al Harassis, sabkhah deposits in Umm as Samim, aeolian sands in the Rub' al Khali), providing independent confirmation of archaeological absence in these contexts. Research campaigns contributed high-intensity coverage of the Dhofar Nejd plateau and adjacent regions, where the relationship between site density and raw material proximity is most clearly expressed[83]. The combination helps document both presence and absence of Palaeolithic occupation across diverse surface geologies.

5. Spatial modelling of human occupation potential

5.1 Water source reconstruction

The drainage network was obtained from the HydroRIVERS dataset of the HydroSHEDS database[64], cropped to the boundaries of Oman and filtered to include only rivers with a total upstream area of at least 1,000 km^2, following the conservative threshold adopted by Breeze et al.[6] for identifying major drainage systems. Rivers were buffered based on their Strahler stream order to estimate channel width, using an exponential function derived from global river width observations[65].

5.2 Distance-to-water analysis

The spatial relationship between archaeological sites and modelled water features was quantified by calculating the Euclidean distance from each site to the nearest water feature (buffered rivers). A kernel density estimate of observed distances was computed to characterise the empirical distance-decay pattern.

To assess whether the observed distance distribution differed from random expectation, a Monte Carlo simulation was performed. For each of 999 iterations, a set of random points equal in number to the observed sites was generated within the Oman study area. Distances to the nearest water feature were calculated for each simulated point set and converted to kernel density estimates. Density values from all iterations were interpolated onto a shared distance axis, producing an ensemble of simulated distance-decay curves. At each distance increment, a 95% confidence envelope was calculated from the ensemble and compared to the observed curve. This approach provides a non-parametric assessment of site–water relationships while accounting for the geometry of the study area and the spatial distribution of water resources (Fig. S5).

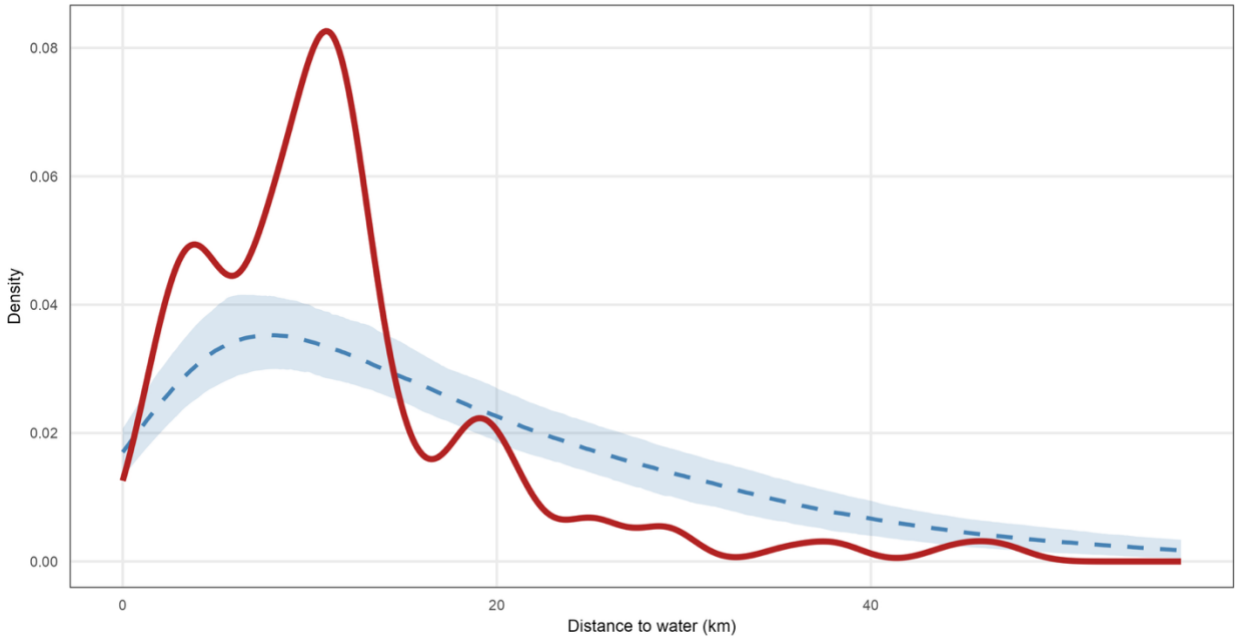

Fig. S5 | Density distribution of distance to water from known MP/MSA sites in Oman (n = 301; solid red line) compared with 95% Monte Carlo confidence interval (blue dashed line and shading) expected under a spatially random null distribution. The observed density exceeds the envelope between approximately 2 and 15 km and falls below it beyond approximately 20 km, indicating that sites occur closer to modelled water than expected under the null.

5.3 Raw material probability modelling (Oman)

In Oman, where the survey campaigns provided systematic records of raw-material presence versus absence, the spatial probability of knappable raw material occurrence was modelled as a function of geological context using a Weights-of-Evidence (WoE) approach[89]. Raw material occurrences were compiled from a dataset of surveyed localities with noted raw material presence (see above). Raw material occurrences were rasterised onto a common analysis grid, producing a binary event raster (presence/absence of raw material occurrence).

Geological polygon data (1:250,000 mapping)[88] were converted to the common raster grid and classified by stratigraphic subseries (or series/system where subseries data were unavailable). Each geological unit was transformed into a binary evidence raster. Positive and negative weights were calculated following standard WoE formulations: positive weights quantify the strength of spatial association between raw material occurrences and the presence of a given geological unit; negative weights quantify the association with its absence. Weights were computed as the natural logarithm of the ratio between conditional probabilities, with a constant of 1e-9 included to prevent undefined values in cases of zero counts.

Binary geological evidence rasters were multiplied by their corresponding positive weights and summed across all units to produce a continuous predictive score surface representing combined geological favourability for raw material occurrence. The summed log-odds surface was

transformed using a logistic function to create a continuous probability surface bounded between 0 and 1.

The association between MP/MSA sites and predicted raw material probability was assessed using the same Monte Carlo framework described above. Predicted probabilities were sampled at known site locations and compared against an ensemble of 999 random point sets. A 95% confidence envelope was calculated at each probability increment to test whether sites occur in areas of higher modelled raw material probability than expected by chance (Fig. S6).

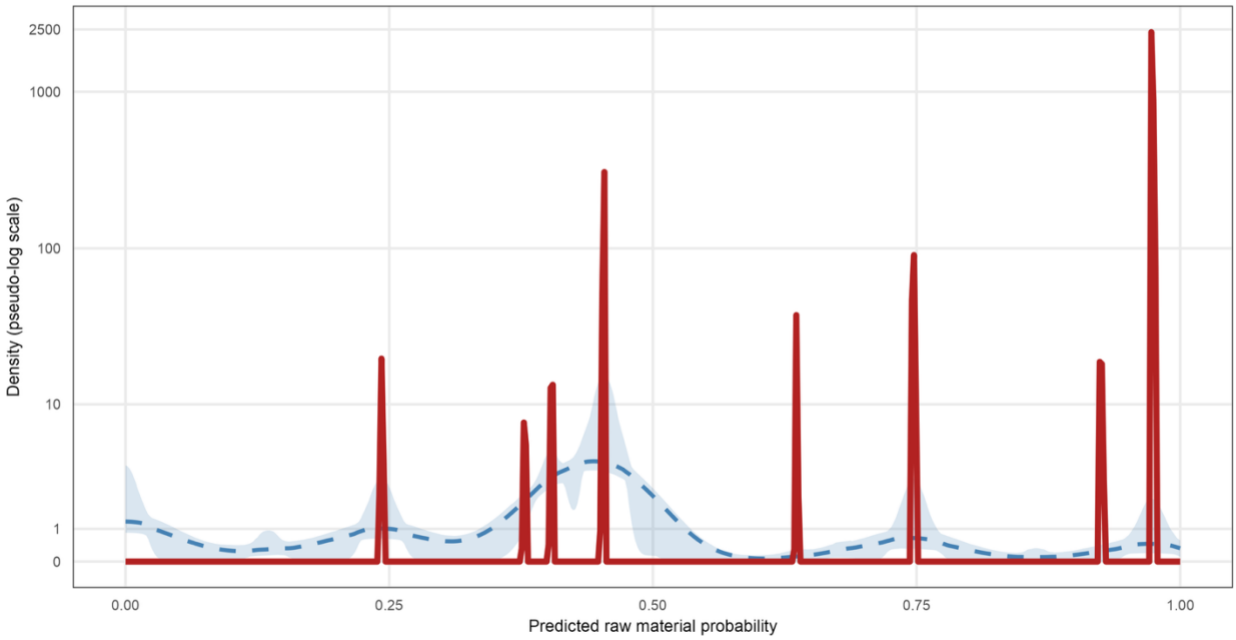

Fig. S6 | Density distribution of raw material probabilities (pseudo-log scale) at known MP/MSA sites in Oman (n = 301; solid red line) compared with 95% Monte Carlo confidence interval (blue dashed line and shading) expected under a spatially random null distribution. The Weights-of-Evidence surface takes a limited set of discrete values, so the observed density appears as narrow peaks at those values rather than as a continuous curve. Sites are concentrated in geological contexts with the highest modelled raw material probabilities.

5.4 Combined human occupation potential model (Oman)

Human occupation potential was classified independently for each resource layer before combination. Water-based potential was defined using empirically derived distance thresholds corresponding to the 50th, 75th, and 95th percentiles of observed site-to-water distances within the Oman data set, producing three classification bands (high, medium, and low potential). All modelled water features were reprojected into UTM Zone 40N for accurate distance buffering. Raw material potential was classified as high, medium, or low by K-means clustering of the modelled WoE probabilities at known MP/MSA site locations. Clustering was used in preference

to fixed percentile thresholds because the probability distribution is strongly right-skewed, such that all percentiles above the 25th returned the same value.

The two layers were combined into a single human occupation potential surface by multiplying together the water-based potential and raw material availability-based potential. Both scales for human occupation potential range from 1 (low potential) to 3 (high potential), so the combined human occupation potential ranges from 0 to 9. Unlike additive methods, this approach ensures that a high value in one parameter cannot fully compensate for a deficiency in the other, thereby prioritising locations where both resources are simultaneously accessible. The combined surface was subsequently reclassified as follows: low potential (values 1-3) represents areas where at least one resource is at its minimum, or both are low; medium potential (values 4 and 6) represents locations where both resources are mid-range or one is high but the other mid-range; and high potential (value 9) represents locations where both resources are high. Because the combination is multiplicative, values of 5, 7, and 8 do not occur.

Validation of the combined model followed the Monte Carlo approach described above. For each of 999 iterations, modelled human occupation potential values were sampled at random locations within the study area, equal in number to the known sites, and expressed as proportions across the potential classes. The 95% confidence envelope from the ensemble of simulated distributions was compared to the observed distribution of potential values at known MP/MSA sites in Oman (Extended Data Fig. 1d). Further validation of the combined model compared two logistic regression models: a baseline model based on water proximity alone and a full model that added raw material availability. Known archaeological site locations were paired with a set of randomly generated background points (n = 10 x known site count) sampled from the study extent with a 100-m buffer around known sites to avoid pseudo-absences. Water-based potential values and raw material availability-based potential values for Oman were independently extracted at each site and background location. Discriminative performance of each model was evaluated using the area under the receiver operating characteristic curve (AUC) (Fig. S7).

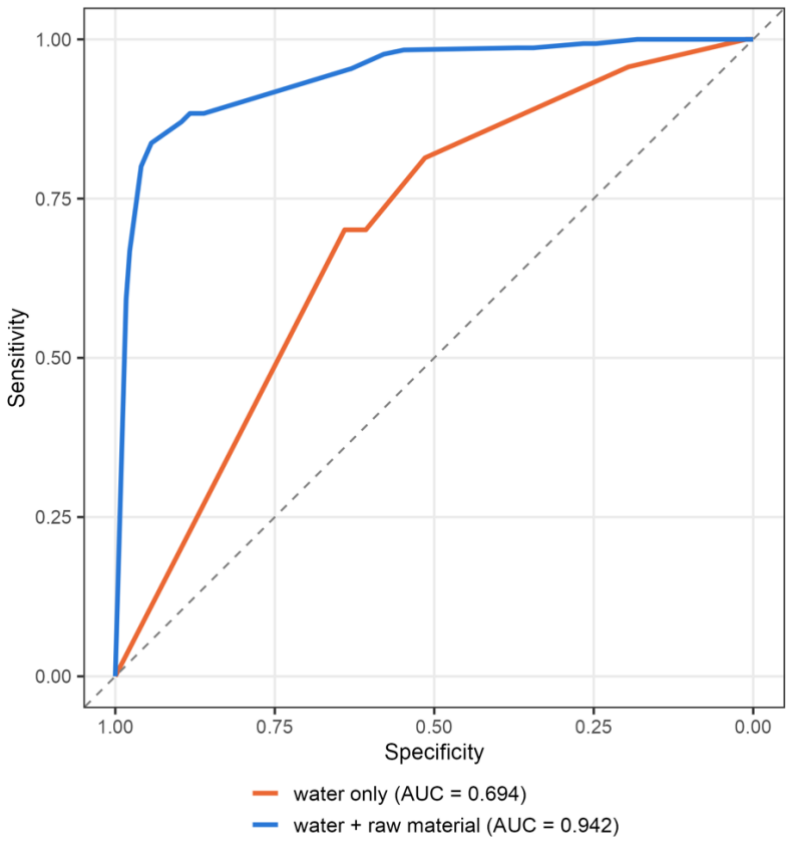

Fig. S7 | Model discrimination for MP/MSA site presence in Oman. Receiver operating characteristic (ROC) curves comparing classification performance using water-based potential only (red line, AUC = 0.694) and water- and raw material availability-based potentials together (blue line, AUC = 0.942). The addition of raw material availability significantly improves predictive accuracy (DeLong's test, $p < 0.05$). The dashed grey line represents chance-level performance (AUC = 0.50).

5.5 Human occupation potential for the Arabian Peninsula

Human occupation potential for the entire Arabian Peninsula was classified following a similar approach as described for Oman. Water availability potential was defined using empirically derived distance thresholds corresponding to the 50th, 75th, and 95th percentiles of observed site-to-water distances within the Peninsula-wide data set, producing three classification bands (high, medium, and low potential). Due to the current lack of data on estimated extents for palaeolakes, water sources were limited to the HydroRIVERS drainage network, filtered to include only rivers with a total upstream area of at least 1,000 km^2 and to exclude modelled rivers in areas mapped with Quaternary aeolian deposits, following methods outlined by Breeze et al.[6].

Raw material availability was classified by the presence or absence of raw material resources in particular geological contexts. Surface geology was derived from the USGS digital geological map of Arabia, which was digitised from the 1:2,000,000-scale USGS–Arabian American Oil Company

Geologic Map of the Arabian Peninsula[62]. The original paper maps were traced onto mylar, scanned at 300 dpi, vectorised through ARC/INFO, and projected in Lambert Conformal Conic with an RMS error not exceeding 0.5 mm at source scale, equivalent to ~1 km on the ground. Polygons in the digital dataset are attributed only by generalised geological age (e.g. Tertiary, Cretaceous, Quaternary) without subdivision into formations or members. To enable raw material classification at the formation level, the original 1:2,000,000 source map[63] was reclassified for each generalised age polygon by its constituent lithostratigraphic units, using the formation descriptions and map legends of the original source sheets, supplemented by published stratigraphic summaries[29,30,90].

Each classified formation was then assessed for the presence or absence of knappable raw materials based on published lithological descriptions and, where available, field verification from the Rub' al Khali crossing expedition and 44 Oman survey campaigns (Supplementary Information Section 4). Formations were classified as containing workable raw material if accounts document the occurrence of any of the following cryptocrystalline or fine-grained lithologies exhibiting conchoidal fracture: chert, chalcedony, quartzite, vein quartz, rhyolite, or silicified limestone/sandstone. Formations described as comprising exclusively carbonates, evaporites, marls, loose siliciclastic sediments, or coarse-grained crystalline rocks without reported siliceous components were classified as lacking knappable material. This classification is necessarily conservative at the Peninsula scale, as some formations that are mapped as lacking raw material at 1:2,000,000 resolution may contain localised siliceous occurrences not captured at that scale; conversely, the presence of a formation containing chert does not guarantee surface availability in all mapped areas. In contrast to the Weights-of-Evidence probability model used for Oman (Section 5.3), the Peninsula-wide raw-material layer follows a binary classification: each formation was assigned a value of 1 where knappable raw materials are documented and 0 where they are absent. Bedrock geology and drainage layers were then combined (Fig. 2a) using the same multiplicative approach as in the Oman dual-resource model (Extended Data Fig. 1c). Because raw-material availability is coded as presence and absence, the final model of human occupation potential is effectively limited to where raw materials are present and scaled by proximity to water resources.

Validation of the combined model followed the Monte Carlo approach described above. For each of 999 iterations, modelled human occupation potential values were sampled at random locations within the study area, equal in number to the known sites, and expressed as proportions across the potential classes. The 95% confidence envelope from the ensemble of simulated distributions was compared to the observed distribution of potential values at known MP/MSA sites (Fig. 2b). Further validation of the combined model compared two logistic regression models following the AUC approach described above. A baseline water-only model was compared to a combined water and raw material model to assess whether including raw material availability improves prediction of the location of archaeological sites (Extended Data Fig. 2).

5.6 Software

All spatial analyses were conducted in R (version 4.5.2) using the terra (version 1.9-50)[91] and sf (version 1.1-1)[92] packages. Receiver operating characteristic curves, area under the curve values, and DeLong's tests were computed with pROC (version 1.19.0.1)[93,94], and maps were produced in R (version 4.5.2) and QGIS (version 3.28). Weights-of-Evidence modelling of raw material probability was implemented directly in R, computing positive and negative weights from cell counts of raw material presence and absence within each mapped geological category. Drainage data were obtained from HydroSHEDS (https://www.hydrosheds.org)[64]. Geological mapping for Oman follows the 1:250,000 geological mapping of Oman[88]; Peninsula-scale geology follows Bramkamp et al.[63] via the USGS digital compilation[62]. The modular structure of the workflow (geological classification of raw material potential, independent water proximity modelling, multiplicative combination, and Monte Carlo validation) is adaptable to other regions with suitable geological and hydrological data.

6. Chronology of palaeolakes and archaeological sites

Fig. 1b displays OSL ages from lacustrine deposits in the central Rub' al Khali, derived from Matter et al.[16], as well as from documented Middle Palaeolithic (MP) and Middle Stone Age (MSA) sites surrounding the Rub' al Khali. Throughout the manuscript, the term MSA is used to designate assemblages of African affinity and MP for those of western Asian affinity; MP/MSA denotes Peninsula-wide scope.

Locations of geological investigation during the survey correspond to palaeolake sites 14.3, 14.7, 15.1, and 15.3 from the Saudi Arabian portion of the Rub' al Khali. The dated sites span three distinct humid phases: Site 14.3 (three samples: 122 ± 6 ka, 118 ± 10 ka, 111 ± 9 ka) corresponds to MIS 5e–5d; Sites 15.1 and 15.3 (107 ± 13 ka, 96 ± 6 ka) correspond to MIS 5c; and Site 14.7 (67 ± 9 ka) corresponds to MIS 5a–MIS 4. Error bars represent 1σ uncertainties. Points are plotted at mean ages with horizontal error bars extending to ±1σ. Site labels (14.3, 14.7, 15.1, 15.3) correspond to original designations in Matter et al.[16].

Published chronometric ages from MP/MSA archaeological sites in the Arabian Peninsula evidence early human habitation at the margins of the desert: Jebel Faya (UAE), Al Kharj (central Saudi Arabia), Mundafan (western Rub' al Khali margin), and Dhofar Nejd (southern Rub' al Khali margin). These represent potential source populations for interior settlement.

Jebel Faya (United Arab Emirates)

Site FAY-NE1 at Jebel Faya (25.12°N, 55.85°E) is a rock shelter containing a stratified Palaeolithic sequence extending back to ~210 ka[23]. Older MP horizons (Assemblages D/VII and E/VIII) document occupation during MIS 7 and MIS 6 but are omitted from Fig. 1b, which plots only the MIS 5 interval relevant to the interior palaeolake chronology. Four MSA horizons from this interval are plotted: Assemblage C (125 ± 10 ka), Archaeological Horizon (AH) VI (134 ± 7 ka), AH V (123 ± 10 ka), and AH II (80 ± 5 ka). Ages are based on single-grain OSL dating of quartz from sandy sediments directly associated with lithic assemblages[17,18,23].

Al Kharj / Umm al Sha'al (Central Saudi Arabia)

Site AK-31 at Umm al Sha'al in the Al Kharj region (24.08°N, 47.29°E) preserves stratified MP/MSA deposits associated with palaeolake sediments[19]. Three OSL ages from the excavated sequence are included: 87 ± 10 ka, 81 ± 9 ka, and 71 ± 6 ka, spanning MIS 5b–a.

Mundafan (Western Rub' al Khali Margin)

The Mundafan palaeolake basin (18.52°N, 45.35°E) preserves MP surface scatters associated with lacustrine shoreline deposits[10,11]. Although most lithic material occurs as surface scatters, site MDF-61 yielded stratified deposits dated by OSL. Four ages are plotted from the excavated sequence: 95.6 ± 5.9 ka, 89.7 ± 8.0 ka, 84.7 ± 8.9 ka, and 77.1 ± 8.0 ka (OSL samples 19, 14, 10, and 8 respectively).

Dhofar Nejd (Southern Oman)

The Nejd plateau of Dhofar, southern Oman (~17-18°N, 53-54°E), preserves an extensive distribution of MSA sites[83]. Ten OSL ages from four stratified sites are included: Aybut Auwal (TH59: two ages, 106 ± 9 ka and 107 ± 9 ka), Aybut Hills 5 (TH505: two ages, 106.2 ± 6.3 ka and 106.5 ± 6.4 ka), Aybut Hills 6 (TH584: five ages ranging from 95.3 ± 5.7 ka to 101.3 ± 6.0 ka), and Upper Amut 1 (TH571: one age, 104.5 ± 7.1 ka). Bayesian phase modelling of all ages yields a combined estimate of 109–95 ka (95% CI; mean 102 ± 3 ka), constraining the Dhofar Nubian industry to MIS 5c[5,20].

Table S4. Chronometric ages for MP/MSA archaeological sites in Arabia plotted in Fig. 1b.

Site	Sample/Layer	Age (ka)	±1σ (ka)	Method	Region	Reference
Aybut Auwal	TH59-1	106	9	OSL	Dhofar Nejd	[20]
Aybut Auwal	TH59-2	107	9	OSL	Dhofar Nejd	[20]
Aybut Hills 5	TH505-1	106.2	6.3	OSL	Dhofar Nejd	[5]
Aybut Hills 5	TH505-2	106.5	6.4	OSL	Dhofar Nejd	[5]
Aybut Hills 6	TH584-1	95.3	5.7	OSL	Dhofar Nejd	[5]
Aybut Hills 6	TH584-2	100.8	6.4	OSL	Dhofar Nejd	[5]
Aybut Hills 6	TH584-3	99.9	5.5	OSL	Dhofar Nejd	[5]
Aybut Hills 6	TH584-4	101.3	6	OSL	Dhofar Nejd	[5]
Aybut Hills 6	TH584-5	100.6	5.7	OSL	Dhofar Nejd	[5]
Upper Amut 1	TH571	104.5	7.1	OSL	Dhofar Nejd	[5]
Mundafan Al-Buhayrah	MDF-61 OSL19	95.6	5.9	OSL	Mundafan	[11]
Mundafan Al-Buhayrah	MDF-61 OSL14	89.7	8	OSL	Mundafan	[11]
Mundafan Al-Buhayrah	MDF-61 OSL10	84.7	8.9	OSL	Mundafan	[11]
Mundafan Al-Buhayrah	MDF-61 OSL8	77.1	8	OSL	Mundafan	[11]
Umm al Sha'al	AKE31-3	87	10	OSL	Al Kharj	[19]
Umm al Sha'al	AKE31-4	71	6	OSL	Al Kharj	[19]
Umm al Sha'al	AKE31-5	81	9	OSL	Al Kharj	[19]
Jebel Faya	Assemblage C	125	10	OSL	Jebel Faya	[17]
Jebel Faya	AH VI	134	7	OSL	Jebel Faya	[23]
Jebel Faya	AH V	123	10	OSL	Jebel Faya	[23]
Jebel Faya	AH II	80	5	OSL	Jebel Faya	[18]

7. Colonisation dynamics in dual-resource landscapes

The systematic absence of archaeologically visible MP/MSA remains from the Rub' al Khali interior, despite abundant freshwater evidence and contemporary human presence at the desert margins, invites consideration of complementary explanations beyond the dual-resource pattern documented in the main text.

*Demographic factors***.** Human dispersal across the Arabian Peninsula was, like other Pleistocene dispersals, likely a complex, historically contingent process influenced by multiple factors[56,95]. If MP/MSA populations dispersing into Arabia were small, as might be expected for colonising human foragers entering unfamiliar territory[54,55], then settlement in a favourable region with sufficient resources, such as the dual-resource zones of Dhofar or the western Rub' al Khali margin, may not have generated sufficient demographic pressure to push groups into neighbouring regions lacking essential resources. In this scenario, foragers were 'pulled' into attractive dual-resource zones rather than 'pushed' into the interior[56].

*Landscape knowledge***.** It is unlikely that MP/MSA populations were simply unaware of the Rub' al Khali interior over the ~50-thousand-year span of documented margin occupation. Foragers actively accumulate and transmit landscape knowledge[57,58], and such knowledge would have been especially important for reducing risk and uncertainty among human groups colonising the Arabian Peninsula[59,60]. Knowledge of the interior's lack of knappable raw material may itself have functioned as a deterrent, reinforcing the pull of dual-resource zones at the margins.

*Potential for future discoveries***.** It remains possible that future fieldwork may document small logistical, exploratory, or resource procurement sites in the Rub' al Khali interior. However, the systematic pattern of absence documented across 55 palaeolake localities spanning the full extent of the ~1,500 km transect, combined with >95% ground visibility and the confirmed absence of knappable raw materials throughout the interior basin, indicates that any such discoveries would represent exceptional or low-intensity events against a broader pattern of archaeologically visible absence.

Terrain roughness and ecological diversity. Rugged terrain has been identified as a predictor of hominin site location at continental scale, on the reasoning that slopes place microclimates and ecotones in close proximity and so support higher biome diversity and a wider range of food resources. Across Africa and Eurasia over the past three million years, roughness contributes more to biome diversity at hominin locations than either temperature or precipitation[61]. Documented MP/MSA sites in Arabia are consistent with this pattern, occupying rougher terrain than background locations, with median roughness of 5.44 m against 3.47 m, although the effect is small (Cliff's delta = 0.197; Extended Data Fig. 4a). Two considerations limit direct comparison. The measures differ in definition and in scale, roughness here being the elevation range within a 3 x 3 neighbourhood at 104 m resolution, expressed in metres, against a mean topographic gradient in metres per metre averaged over 0.5 degree grid cells, some three orders of magnitude coarser.

The ecological mechanism itself cannot be evaluated for Arabia, since no transient palaeo-productivity or biome reconstruction exists at a resolution comparable to the survey data. What can be tested is whether roughness carries predictive information independent of the two resources modelled here. Adding roughness to the combined water and raw material model reduces discrimination from an area under the curve of 0.762 to 0.738 (DeLong $Z = 8.99$, $P < 2.2 \times 10^{-16}$), and its coefficient in the full model is negative and small in magnitude (beta = -0.0062, P = 0.043). Knappable lithologies occur disproportionately on low-relief ground (Spearman's rho = -0.217; Extended Data Fig. 4b), so roughness is not a proxy for lithic access in Arabia either. The association between roughness and site location is largely absorbed by water proximity. Whether ecological diversity operated as an additional influence at the basin margins remains open, and the relationship between environmental heterogeneity and resource availability that it would require is the avenue for further work.

8. Future research and strategies

Several of the constraints on this study point to specific and tractable next steps. (1) The chronology presented here rests on regional correlation rather than direct dating, because the fieldwork was conducted under a non-collecting protocol. Luminescence sampling of the surveyed lacustrine sections would allow the interior lake phases to be dated independently and would test whether the correlation to the MIS 5 highstands holds across the full transect. (2) Mollusc identifications reported here were made from field photographs, and the assemblages were not collected. Systematic sampling would permit assemblage-level analysis, which is considerably more informative for palaeosalinity and palaeoecology than the presence or absence of individual taxa, and would allow the water chemistry of the interior lakes to be characterised rather than inferred. (3) The transect crosses the interior from west to east, and the raw-material record at its ends is necessarily limited to the localities it intersects. Extending survey coverage around the western and northern margins of the Rub' al Khali would test the margin-restricted distribution of knappable stone reported here against a wider sample, and would establish whether the dual-resource zones identified at the transect termini are continuous or discrete. (4) The Peninsula-wide model treats raw-material presence as binary and weights all lithologies equally. Incorporating nodule size, fracture quality, abundance and surface availability would refine the habitability estimate, although doing so would require systematic raw-material survey at a scale not currently available. (5) The model identifies where water and knappable stone co-occurred, but not whether those patches were reachable from one another within a single humid phase. Least-cost path analysis, travel-time thresholds or graph-based measures of network structure would allow the lithic archipelago to be assessed as a mobility network rather than as a distribution of isolated patches.

9. References

1. Timmermann, A. & Friedrich, T. Late Pleistocene climate drivers of early human migration. *Nature* **538**, 92–95 (2016).
2. Beyer, R. M., Krapp, M., Eriksson, A. & Manica, A. Climatic windows for human migration out of Africa in the past 300,000 years. *Nat. Commun.* **12**, 4889 (2021).
3. Breeze, P. S. *et al.* Palaeohydrological corridors for hominin dispersals in the Middle East∼ 250–70,000 years ago. *Quat. Sci. Rev.* **144**, 155–185 (2016).
4. Groucutt, H. S. *et al.* Multiple hominin dispersals into Southwest Asia over the past 400,000 years. *Nature* **597**, 376–380 (2021).
5. Rose, J. I. *et al.* A failed human expansion out of Africa 100,000 years ago. *Prepr. Httpsdoi Org1021203rs* **3**, (2026).
6. Breeze, P. S. *et al.* Remote sensing and GIS techniques for reconstructing Arabian palaeohydrology and identifying archaeological sites. *Quat. Int.* **382**, 98–119 (2015).
7. Rosenberg, T. *et al.* Humid periods in southern Arabia: windows of opportunity for modern human dispersal. *Geology* **39**, 1115–1118 (2011).
8. Rosenberg, T. M. *et al.* Middle and Late Pleistocene humid periods recorded in palaeolake deposits of the Nafud desert, Saudi Arabia. *Quat. Sci. Rev.* **70**, 109–123 (2013).
9. Nicholson, S. L. *et al.* Pluvial periods in Southern Arabia over the last 1.1 million-years. *Quat. Sci. Rev.* **229**, 106112 (2020).
10. Crassard, R. *et al.* Middle Palaeolithic and Neolithic occupations around Mundafan palaeolake, Saudi Arabia: implications for climate change and human dispersals. *PLoS One* **8**, e69665 (2013).
11. Groucutt, H. S. *et al.* Human occupation of the Arabian empty quarter during MIS 5: evidence from Mundafan Al-Buhayrah, Saudi Arabia. *Quat. Sci. Rev.* **119**, 116–135 (2015).
12. Kuhn, S. L. *The Evolution of Paleolithic Technologies*. (Routledge, 2020).
13. Kuhn, S. L. Neanderthal technoeconomics: an assessment and suggestions for future developments. *Neanderthal Lifeways Subsist. Technol. One Hundred Fifty Years Neanderthal Study* 99–110 (2011).
14. Muller, A. & Clarkson, C. Identifying major transitions in the evolution of lithic cutting edge production rates. *PLoS One* **11**, e0167244 (2016).
15. McClure, H. Radiocarbon chronology of late Quaternary lakes in the Arabian Desert. *Nature* **263**, 755–756 (1976).
16. Matter, A., Neubert, E., Preusser, F., Rosenberg, T. & Al-Wagdani, K. Palaeo-environmental implications derived from lake and sabkha deposits of the southern Rub'al-Khali, Saudi Arabia and Oman. *Quat. Int.* **382**, 120–131 (2015).
17. Armitage, S. J. *et al.* The southern route "out of Africa": evidence for an early expansion of modern humans into Arabia. *Science* **331**, 453–456 (2011).

18. Bretzke, K. *et al.* Archaeology, chronology, and sedimentological context of the youngest Middle Palaeolithic assemblage from Jebel Faya, United Arab Emirates. *Archaeol. Anthropol. Sci.* **17**, 60 (2025).
19. Crassard, R., Hilbert, Y. H., Preusser, F., Wulf, G. & Schiettecatte, J. Middle Palaeolithic occupations in central Saudi Arabia during MIS 5 and MIS 7: new insights on the origins of the peopling of Arabia. *Archaeol. Anthropol. Sci.* **11**, 3101–3120 (2019).
20. Rose, J. I. *et al.* The Nubian complex of Dhofar, Oman: an African middle stone age industry in southern Arabia. *PloS One* **6**, e28239 (2011).
21. Usik, V. I., Rose, J. I., Hilbert, Y. H., Van Peer, P. & Marks, A. E. Nubian Complex reduction strategies in Dhofar, southern Oman. *Quat. Int.* **300**, 244–266 (2013).
22. Groucutt, H. S. *et al.* Homo sapiens in Arabia by 85,000 years ago. *Nat. Ecol. Evol.* **2**, 800–809 (2018).
23. Bretzke, K. *et al.* Multiple phases of human occupation in Southeast Arabia between 210,000 and 120,000 years ago. *Sci. Rep.* **12**, 1600 (2022).
24. Merrick, H. V. & Brown, F. H. Obsidian sources and patterns of source utilization in Kenya and northern Tanzania: some initial findings. *Afr. Archaeol. Rev.* **2**, 129–152 (1984).
25. Spinapolice, E. E. Raw material economy in Salento (Apulia, Italy): new perspectives on Neanderthal mobility patterns. *J. Archaeol. Sci.* **39**, 680–689 (2012).
26. Nash, D. J., Coulson, S., Staurset, S., Smith, M. P. & Ullyott, J. S. Provenancing silcrete in the Cape coastal zone: implications for Middle Stone Age research in South Africa. *J. Hum. Evol.* **65**, 682–688 (2013).
27. Brooks, A. S. *et al.* Long-distance stone transport and pigment use in the earliest Middle Stone Age. *Science* **360**, 90–94 (2018).
28. Herrero-Alonso, D. *et al.* Neanderthal mobility over very long distances: The case of El Castillo cave (northern Spain) and the 'Vasconian'Mousterian. *J. Hum. Evol.* **205**, 103715 (2025).
29. Edgell, H. S. *Arabian Deserts: Nature, Origin, and Evolution*. (Springer, 2006).
30. Stewart, S. Structural geology of the Rub'Al-Khali Basin, Saudi Arabia. *Tectonics* **35**, 2417–2438 (2016).
31. Kazak, E. S., Al Gaoud, A., Ahmed, S. M., Souid, F. & Nabi, A. Origin of Umm Al Heesh lake in the Rub'Al Khali desert, Saudi Arabia. *Sci. Rep.* **15**, 34850 (2025).
32. Clark-Wilson, R. *et al.* Assessing the intensity of Late Quaternary humid phases in the Nefud Desert, northern Arabia. *J. Quat. Sci.* **41**, 207–218 (2026).
33. Zaki, A. S. *et al.* Monsoonal imprint on late Quaternary landscapes of the Rub'al Khali Desert. *Commun. Earth Environ.* **6**, 255 (2025).
34. Petraglia, M. D., Groucutt, H. S., Guagnin, M., Breeze, P. S. & Boivin, N. Human responses to climate and ecosystem change in ancient Arabia. *Proc. Natl. Acad. Sci.* **117**, 8263–8270 (2020).
35. Scerri, E. *et al.* Neolithic pastoralism in marginal environments during the Holocene wet phase, northern Saudi Arabia. *Antiquity* **92**, (2018).

36. Maiorano, M. P. *et al.* Living and moving in Maitan. *Proc. Semin. Arab. Stud.* **50**, 83–100 (2020).
37. Petraglia, M. D. *et al.* Hominin dispersal into the Nefud desert and Middle Palaeolithic settlement along the Jubbah palaeolake, northern Arabia. *PLoS One* **7**, e49840 (2012).
38. Groucutt, H. S. *et al.* Middle Palaeolithic raw material procurement and early stage reduction at Jubbah, Saudi Arabia. *Archaeol. Res. Asia* **9**, 44–62 (2017).
39. Chlachula, D. *et al.* Evidence of Middle Palaeolithic human occupation in south-central Oman. *Antiquity* **99**, e9 (2025).
40. Eren, M. I. *et al.* Examining the distribution of Middle Paleolithic Nubian cores relative to chert quality in southern (Nejd, Dhofar) and south-central (Duqm, Al Wusta) Oman. *Geoarchaeology* **40**, e22019 (2025).
41. Cancellieri, E., Cremaschi, M., Zerboni, A. & Di Lernia, S. Climate, environment, and population dynamics in Pleistocene Sahara. in *Africa from MIS 6-2: Population Dynamics and Paleoenvironments* 123–145 (Springer, 2016).
42. Yang, Z. *et al.* Terminal Pleistocene Human Occupation of the Qomolangma Region: New Evidence from the Su-re Site. *Land* **13**, 1064 (2024).
43. Leplongeon, A., Bailly, M. & Graff, G. Raw-material exploitation in the earlier and middle stone age in the Eastern Desert of Egypt: evidence from Wadi Abu Subeira. *Antiquity* **98**, e13 (2024).
44. Van Peer, P., Vermeersch, P. M. & Paulissen, E. *Chert Quarrying, Lithic Technology and a Modern Human Burial at the Palaeolithic Site of Taramsa 1, Upper Egypt*. vol. 5 (Leuven university press, 2010).
45. Will, M. *et al.* Specialised and persistent raw material procurement by humans in the Middle Pleistocene. *Nat. Commun.* **17**, 2702 (2026).
46. Miller, G. L. *et al.* Hunter-gatherer gatherings: Stone-tool microwear from the Welling Site (33-Co-2), Ohio, USA supports Clovis use of outcrop-related base camps during the Pleistocene Peopling of the Americas. *World Archaeol.* **51**, 47–75 (2019).
47. Foley, R. A. & Lahr, M. M. Lithic landscapes: Early human impact from stone tool production on the central Saharan environment. *PloS One* **10**, e0116482 (2015).
48. Rose, J. I. *et al.* Lithic miniaturization and technological innovation on the Southern Dispersal Route out of Africa. *J. Paleolit. Archaeol.* **8**, 40 (2025).
49. Field, J. S., Petraglia, M. D. & Lahr, M. M. The southern dispersal hypothesis and the South Asian archaeological record: examination of dispersal routes through GIS analysis. *J. Anthropol. Archaeol.* **26**, 88–108 (2007).
50. Jennings, R. P. *et al.* The greening of Arabia: Multiple opportunities for human occupation of the Arabian Peninsula during the Late Pleistocene inferred from an ensemble of climate model simulations. *Quat. Int.* **382**, 181–199 (2015).
51. Féblot-Augustins, J. Mobility strategies in the late Middle Palaeolithic of central Europe and western Europe: elements of stability and variability. *J. Anthropol. Archaeol.* **12**, 211–265 (1993).

52. Brantingham, P. J. A neutral model of stone raw material procurement. *Am. Antiq.* **68**, 487–509 (2003).
53. Brantingham, P. J. Measuring forager mobility. *Curr. Anthropol.* **47**, 435–459 (2006).
54. Meltzer, D. J. What do you do when no one's been there before? Thoughts on the exploration and colonization of new lands. *First Am. Pleistocene Colon. New World* **27**, 27–58 (2002).
55. Meltzer, D. J. Lessons in landscape learning. in *The Colonization of Unfamiliar Landscapes* 246–262 (Routledge, 2003).
56. Anthony, D. W. Migration in archeology: The baby and the bathwater. *Am. Anthropol.* **92**, 895–914 (1990).
57. Kelly, R. L. Colonization of new land by hunter-gatherers: expectations and implications based on ethnographic data. in *The Colonization of Unfamiliar Landscapes* 68–68 (Routledge, 2003).
58. Hitchcock, R. K., Whallon, R. & Lovis, W. A. Information and its role in hunter-gatherer bands. in (ISD, 2011).
59. Rockman, M. Knowledge and learning in the archaeology of colonization. in *The Colonization of Unfamiliar Landscapes* 27–43 (Routledge, 2003).
60. Meltzer, D. J. 11 Modeling the Initial Colonization of the Americas. *Settl. Am. Cont. Multidiscip. Approach Hum. Biogeogr.* 123 (2004).
61. Zeller, E. & Timmermann, A. The evolving three-dimensional landscape of human adaptation. *Sci. Adv.* **10**, eadq3613 (2024).
62. Pollastro, R. M., Karshbaum, A. S. & Viger, R. J. *Maps Showing Geology, Oil and Gas Fields and Geologic Provinces of the Arabian Peninsula*. (1999).
63. Bramkamp, R. A., Ramirez, L. F., Brown, G. F., Pocock, A. E. & Sander, N. J. Geologic Map of the Arabian Peninsula. (1963).
64. Lehner, B. & Grill, G. Global river hydrography and network routing: baseline data and new approaches to study the world's large river systems. *Hydrol. Process.* **27**, 2171–2186 (2013).
65. Downing, J. A. *et al.* Global abundance and size distribution of streams and rivers. *Inland Waters* **2**, 229–236 (2012).
66. Ho, Y. & Hengl, T. Global Ensemble Digital Terrain Model 30m (GEDTM30). Zenodo https://doi.org/10.5281/ZENODO.18887460 (2026).
67. Matter, A. *et al.* Reactivation of the Pleistocene trans-Arabian Wadi ad Dawasir fluvial system (Saudi Arabia) during the Holocene humid phase. *Geomorphology* **270**, 88–101 (2016).
68. Ismail, N. S. & Arif, A. M. Population dynamics of Melanoides tuberculata (Thiaridae) snails in a desert spring, United Arab Emirates and infection with larval trematodes. *Hydrobiologia* **257**, 57–64 (1993).
69. Aloufi, A. A. & Amr, M. Z. Freshwater Snails of Tabuk Region, Northern Saudi Arabia. *Jordan J. Biol. Sci.* **147**, 1–4 (2015).
70. Ahmed, M. M. Systematic study on mollusca from Arabian gulf and Shatt Al-Arab, Iraq. (1975).

71. Mohammed, H. H., Ahmed, H. K., Al-Taei, S. A. & Ali, M. H. Macro-invertebrates response to acute salinity changes in the Shatt Al-Arab River system, Southern Iraq. *Iraqi J. Aquac.* **17**, 61–78 (2020).
72. Sultan, M. *et al.* Geochemical, isotopic, and remote sensing constraints on the origin and evolution of the Rub Al Khali aquifer system, Arabian Peninsula. *J. Hydrol.* **356**, 70–83 (2008).
73. Elmahdy, S., Ali, T. & Mohamed, M. Regional mapping of groundwater potential in ar rub al khali, arabian peninsula using the classification and regression trees model. *Remote Sens.* **13**, 2300 (2021).
74. Awadh, S. M., Al-Mimar, H. & Yaseen, Z. M. Groundwater availability and water demand sustainability over the upper mega aquifers of Arabian Peninsula and west region of Iraq: SM Awadh et al. *Environ. Dev. Sustain.* **23**, 1–21 (2021).
75. UN-ESCWA, BGR (United Nations Economic and Social Commission for Western Asia; Bundesanstalt für Geowissenschaften und Rohstoffe). *Inventory of Shared Water Resources in Western Asia*. (2013).
76. Munroe, J. S. & Laabs, B. J. Latest Pleistocene history of pluvial lake Franklin, northeastern Nevada, USA. *GSA Bull.* **125**, 322–342 (2013).
77. Schofield, I., Jewell, P., Chan, M., Currey, D. & Gregory, M. Shoreline development, longshore transport and surface wave dynamics, Pleistocene Lake Bonneville, Utah. *Earth Surf. Process. Landf. J. Br. Geomorphol. Res. Group* **29**, 1675–1690 (2004).
78. Rose, J. The question of Upper Pleistocene connections between east Africa and south Arabia. *Curr. Anthropol.* **45**, 551–555 (2004).
79. Rose, J. I. *Among Arabian Sands: Defining the Palaeolithic of Southern Arabia*. (Southern Methodist University, 2007).
80. Rose, J. The Arabian Corridor Migration Model: archaeological evidence for hominin dispersals into Oman during the Middle and Upper Pleistocene. in 219–237 (JSTOR, 2007).
81. Rose, J. I. & Usik, V. I. The "Upper Paleolithic" of South Arabia. in *The evolution of human populations in Arabia: paleoenvironments, prehistory and genetics* 169–185 (Springer, 2009).
82. Hilbert, Y. H. *et al.* Archaeological evidence for indigenous human occupation of Southern Arabia at the Pleistocene/Holocene transition: The case of al-Hatab in Dhofar, Southern Oman. *Paléorient* 31–49 (2015).
83. Rose, J. I. *et al.* Prehistoric settlement patterns in southern Oman from the Lower Palaeolithic to the Neolithic. *Paléorient Rev. Pluridiscip. Préhistoire Protohist. L'Asie Sud-Ouest L'Asie Cent.* 83–108 (2023).
84. Hilbert, Y. *et al.* Terminal Pleistocene and Early Holocene archaeology and stratigraphy of the southern Nejd, Oman. *Quat. Int.* **382**, 250–263 (2015).
85. Rose, J. I. The First Peoples of Oman: Palaeolithic Archaeology of the Nejd Plateau. (2019).
86. Rose, J. I. *et al.* 30,000-year-old geometric microliths reveal glacial refugium in Dhofar, southern Oman. *J. Paleolit. Archaeol.* **2**, 338–357 (2019).
87. Rose, J. I. *et al.* Mapping lateral stratigraphy at Palaeolithic surface sites: A case study from Dhofar, Oman. *J. Archaeol. Sci.* **173**, 106117 (2025).

88. Ministry of Petroleum and Minerals, Directorate General of Minerals. *Geological Map of Oman, scale 1:250,000* (Sultanate of Oman, Muscat, in association with Bureau de Recherches Géologiques et Minières, Orléans, 1986–1993).
89. Duke, C. & Steele, J. Geology and lithic procurement in Upper Palaeolithic Europe: a weights-of-evidence based GIS model of lithic resource potential. *J. Archaeol. Sci.* **37**, 813–824 (2010).
90. Powers, R., Ramirez, L. F., Redmond, C. & Elberg Jr, E. *Geology of the Arabian Peninsula: Sedimentary Geology of Saudi Arabia*. (1966).
91. Hijmans, R. J., Brown, A., Barbosa, A. M., Cordano, E. & Dyba, K. terra: Spatial Data Analysis. 1.9-50 https://doi.org/10.32614/CRAN.package.terra (2020).
92. Pebesma, E. Simple Features for R: Standardized Support for Spatial Vector Data. *R J.* **10**, 439 (2018).
93. Robin, X. *et al.* pROC: an open-source package for R and S+ to analyze and compare ROC curves. *BMC Bioinformatics* **12**, 77 (2011).
94. DeLong, E. R., DeLong, D. M. & Clarke-Pearson, D. L. Comparing the Areas under Two or More Correlated Receiver Operating Characteristic Curves: A Nonparametric Approach. *Biometrics* **44**, 837 (1988).
95. Rockman, M. & Steele, J. *Colonization of Unfamiliar Landscapes: The Archaeology of Adaptation*. (Psychology Press, 2003).